REVIEW

Check for updates

The arylvinylpyrimidine scaffold: a tunable platform for luminescent and optical materials

Sylvain Achelle, ID *[a] Julián Rodríguez-López ID *[b] and Françoise Robin-le Guen[a]

The incorporation of electron-withdrawing pyrimidine rings within π-extended systems allows access to a wide variety of fluorescent push–pull molecules that display emission properties highly sensitive to external stimuli. A suitable design of these compounds leads to interesting materials for a variety of optoelectronic applications. In this context, a vast number of arylvinylpyrimidine-based chromophores have been extensively studied during the last two decades. Along with the main synthetic pathways, this review summarizes the photophysical features of these active compounds having great potential and their most important applications as sensors and luminescence materials.

1. Introduction

Intramolecular charge transfer (ICT) is one of the key elements that govern the properties of organic optical materials.[1,2] ICT occurs when an electron-donating group (D) is linked to an electron-attracting fragment (A) *via* a π-conjugated linker (D–π–A, also called push–pull structures). Such structures are characterized by their color, with absorption bands in the visible spectral range that experience a significant red shift with ICT enhancement. Moreover, some push–pull chromophores exhibit intense photoluminescence and nonlinear optical properties,[1] finding widespread application as fluorescence sensors,[3] emitters for light-emitting devices,[4] organic field effect transistors,[5] photovoltaic materials,[6] two-photon absorption chromophores,[7] and second harmonic generation materials.[8]

The pyrimidine ring is a six membered aromatic heterocycle with two nitrogen atoms at positions 1 and 3. Due to the π-deficient character of this heterocycle, the pyrimidinyl fragments act as electron-withdrawing groups. In the case of pyrimidin-2-yl, pyrimidin-4-yl, and pyrimidin-6-yl derivatives, the two nitrogen atoms are in a conjugated position relative to the

[a]*Univ. Rennes, CNRS, ISCR (Institut des Sciences Chimiques de Rennes) – UMR 6226, F-35000 Rennes, France. E-mail: sylvain.achelle@univ-rennes1.fr*
[b]*Universidad de Castilla-La Mancha, Área de Química Orgánica, Facultad de Ciencias y Tecnologías Químicas, 13071 Ciudad Real, Spain. E-mail: julian.rodriguez@uclm.es*

Sylvain Achelle received his PhD in organic chemistry in 2007 from INSA Rouen (France). After two post-doctoral stays at the Universidad de Castilla-La Mancha (Spain) and Institut Curie (France), he was recruited as associate professor at IUT Lannion, University of Rennes 1, in 2010. He obtained the habilitation to direct research in 2014. His main research topics include the luminescence and nonlinear optical properties of organic and

Sylvain Achelle

organometallic heterocyclic derivatives. He has published 84 scientific articles (h-index: 31 according to the Web of Science) and he is currently associate editor of the journal Dyes & Pigments.

*Julián Rodríguez López studied chemistry at the Universidad Complutense de Madrid (UCM) and obtained his PhD with honors (*cum laude*) in 1990. He was a Fulbright postdoctoral fellow at the University of Texas at Austin for one year, under the supervision of Professor Philip Magnus. After successive positions at the UCM, he joined the Universidad de Castilla-La Mancha at Ciudad Real in 1995, where he is currently full pro-*

Julián Rodríguez-López

fessor in Organic Chemistry. His research focuses on the design and synthesis and self-assembly of novel light-emitting π-conjugated systems in order to control their photophysical properties for various (opto)electronic applications.
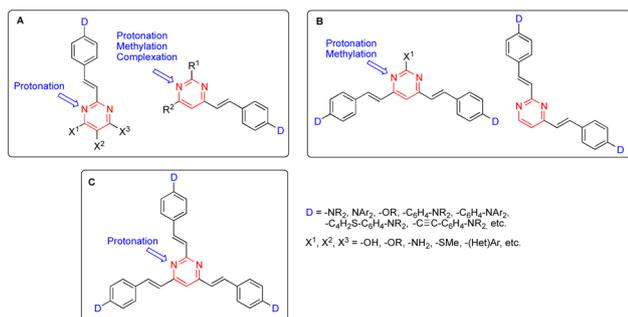
This journal is © The Royal Society of Chemistry 2023

Org. Biomol. Chem., 2023, **21**, 39–52 | **39**

Fig. 1 General structures of 2-arylvinyl and 4-arylvinyl (A), 4,6-bis(aryl-vinyl) and 2,4-bis(arylvinyl) (B), and 2,4,6-tris(arylvinyl)pyrimidines (C).

substituent, making them stronger electron-withdrawing groups than pyridinyl or other diazinyl rings.[9] This electron-withdrawing character can be tuned by engaging the electron lone pairs of the nitrogen atoms upon protonation, complexation, alkylation, or hydrogen bonding. Pyrimidine derivatives substituted with electron-donating fragments through π-conjugated linkers are highly fluorescent and show emission properties highly sensitive to such external stimuli. As a consequence, pyrimidine chromophores are suitable candidates for various optoelectronic applications.[10]

In this context, arylvinylpyrimidine chromophores were intensively studied in the early 2000s. Since then, more than one-hundred linear 2-arylvinyl and 4-arylvinyl, V-shaped 4,6-bis(arylvinyl) and 2,4-bis(arylvinyl), and more recently Y-shaped 2,4,6-tris(arylvinyl)pyrimidines have been designed.[9] In these structures, substituents on the aryl moieties or at different positions on the pyrimidine ring have a significant impact on their photophysical behavior (Fig. 1).

In this review, we will give a general outline of the synthetic methodologies, photophysical properties, and applications of arylvinylpyrimidine chromophores. Coverage of the large number of reported structures is beyond the scope of this

paper and, therefore, special emphasis will be placed on those compounds with the greatest potential.
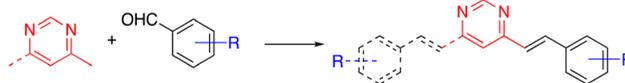
2. Synthetic approaches

The arylvinylpyrimidine scaffold is usually obtained by functionalizing previously formed pyrimidine rings. Although the Suzuki cross-coupling reaction of chloropyrimidines with potassium alkenyltrifluoroborates has been used for their synthesis,[11] the main methodology is the Knoevenagel condensation of aromatic aldehydes with methylpyrimidine derivatives (Scheme 1).

In particular, Vanden Eynde and coworkers developed a methodology based on the use of concentrated aqueous NaOH solution as the solvent and Aliquat 336® as the phase transfer catalyst.[12] The main advantages of this experimental protocol include the wide range of starting materials available in the market, the use of more environmentally friendly conditions in most cases, and the simple process of treatment and purification of the final products, which often consists of a simple recrystallization method. The method is not only straightforward but also rather economical due to the absence of organic solvents.

This approach initially allowed the synthesis of 4-arylvinyl and 4,6-bis(arylvinyl)pyrimidines,[13–15] although it was later extended to the preparation of 2-arylvinylpyrimidines.[16] The products were formed exclusively as E-stereoisomers. The stereochemistry of the double bonds was unambiguously determined from the coupling constant of the vinylic proton in the ^{1}H NMR spectra (^3J(H–H) ≈ 16 Hz).[13,14] This method tolerated a large variety of substituents on the benzaldehyde precursor. When 4-trifluoromethylbenzaldehyde was used, the reaction required a less concentrated NaOH solution to prevent the Cannizzaro side reaction of the aldehyde.[14] On the other hand, formyl-substituted arylvinylpyrimidines could be obtained from 4-(diethoxymethyl)benzaldehyde followed by deprotection of the acetal group.[12b] Bromoderivatives **1** and **2** (Fig. 2) were the key intermediates that could be used for further functionalization by palladium-catalyzed Suzuki–Miyaura or Sonogashira cross coupling reactions.[13,14,17]

Depending on the substituent of the benzaldehyde derivative, it may be necessary to use another base/solvent pair for

Françoise Robin-le Guen received her PhD in organometallic chemistry from the University of Bretagne Occidentale (Brest, France). She is currently full professor at IUT Lannion, University of Rennes 1 and head of the heterocyclic organometallic teams at the Chemical Sciences Institute of Rennes. Her main research topics are focused on the design of π-conjugated heterocyclic and organometallic systems for dye-sensitized solar cells, luminescence and non-linear optics.

Françoise Robin-le Guen

Scheme 1 Synthesis of arylvinylpyrimidines from methylpyrimidines by the Knoevenagel condensation.
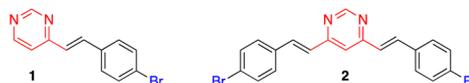
Fig. 2 Structures of bromo-substituted arylvinylpyrimidines **1** and **2**.

40 | *Org. Biomol. Chem.*, 2023, **21**, 39–52

This journal is © The Royal Society of Chemistry 2023

the Knoevenagel condensation, such as KBu^{t}O in THF,[18] KBu^{t}O in DMF,[19] KBu^{t}O without solvent (ground solid),[20] KOH in DMSO,[21] or NaH in THF.[22] In some cases, this reaction was carried out under acidic conditions (HCl in EtOH).[23]

In general, it is difficult to obtain mono-arylvinylpyrimidines starting from 4,6-dimethylpyrimidine.[14,20b] Nevertheless, when the dimethylpyrimidine fragment was embedded in a poly (methyl methacrylate)-based copolymer, surprisingly only mono-condensation products were obtained.[24] On the other hand, the Knoevenagel condensation of 4,6-dimethylpyrimidines with terephthalaldehyde or other dialdehydes allowed access to poly (arylvinylpyrimidine) macromolecules.[25,26]

While 2-methyl-, 4-methyl- and 4,6-dimethylpyrimidine are commercially available and cost-effective chemicals, the accessibility of 2,4-dimethyl- and 2,4,6-trimethylpyrimidine is much more limited. Thus, the preparation of 2,4-bis(arylvinyl) and 2,4,6-tris(arylvinyl)pyrimidines has been approached from 2-chloro-4-methylpyrimidine and 2-chloro-4,6-dimethyl-pyrimidine, respectively, by means of a combination of Suzuki–Miyaura cross coupling and Knoevenagel condensation reactions (Scheme 2).[27] 2,4,6-Tris(arylvinyl)pyrimidines with three different arms could be obtained starting from 2,4-dichloro-6-methylpyrimidine. The higher reactivity of the C4 over the C2 carbon allowed to carry out two Suzuki–Miyaura cross coupling reactions in a sequential manner with excellent selectivity, followed by the Knoevenagel condensation with the corresponding aromatic aldehyde in the methyl group at the C6 position.

Arylvinylpyrimidine derivatives are bench stable compounds in the solid state. Nevertheless, partial reversible protonation could be observed in chlorinated solvents as a result of photogeneration of HCl. Furthermore, some Z/E isomerization was also reported when in the solution was left for a few days.[13,14] Solid state photodimerization has also been reported to give rise to cyclobutane derivatives.[22]

3. Structure–emission property relationships

Due to their more extended π-conjugated linkers, arylvinylpyrimidines exhibit red-shifted absorption and emission relative to their phenylpyrimidine analogues, although the photoluminescence quantum yield (PLQY) is usually lower in moderately polar solvents.[9] They generally must be substituted with strong electron-donating amino groups to show significant emission. Nevertheless, alkoxy-substituted arylvinylpyrimidines are also highly emissive.[9] The emission properties of a series of dimethylamino-substituted styrylpyrimidines are presented in Fig. 3. 4-(p-N,N-Dimethylaminostyryl)pyrimidine **3** displays cyan emission with moderate PLQY ($\Phi_F = 0.15$) in CH$_2$Cl$_2$. When the pyrimidine was substituted at position 2 (compound **4**) instead of position 4, a blue shift of emission was observed with a dramatic decrease in the PLQY. In contrast, a bathochromic shift of emission to green with a significant increase of the PLQY was observed for the 4,6-disubstituted pyrimidine **5**. The emission of 2,4,6-stryrylpyrimidine **6** was further red-shifted but with a slightly lower PLQY than compound **5**. The extension of the π-conjugated linker between the pyrimidin-4-yl fragment and the dimethylamino group on chromophores **7**, **8**, and **9** caused a significant bathochromic shift in the emission and an increase in the PLQY relative to **3**.

The PLQY of 2,4,6-tris(arylvinyl)pyrimidines is highly dependent on the nature of the substituent on the C2 arm.[27] In the diphenylamino series (Fig. 4), compound **9a** exhibited similar photoluminescence properties (λ_{em}, PLQY) as 4,6-distyrylpyrimidine **10** in CH$_2$Cl$_2$. When the C2 arm contained a stronger electron-donating dimethylamino group (**9b**), a red-shifted emission was observed with a dramatic decrease in the
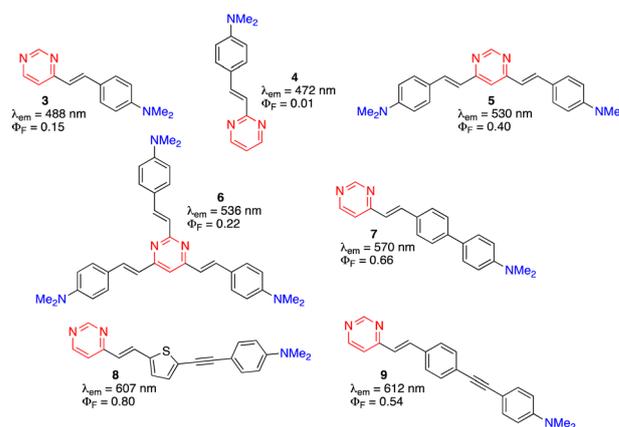

Fig. 3 Structures and emission properties of dimethylamino-substituted styrylpyrimidines **3–9** in CH$_2$Cl$_2$.[13,14,17,27,28]
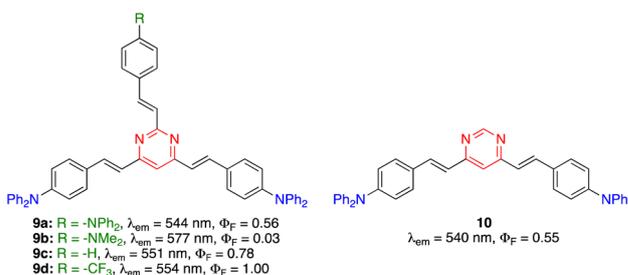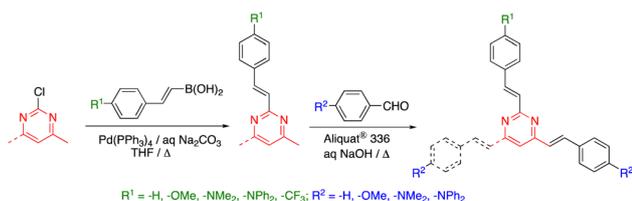

Fig. 4 Structures and photophysical properties of diphenylamino-substituted styrylpyrimidines **9** and **10** in CH$_2$Cl$_2$.[27]

Scheme 2 Synthesis of 2,4-bis(arylvinyl) and 2,4,6-tris(arylvinyl) pyrimidines.

This journal is © The Royal Society of Chemistry 2023

Org. Biomol. Chem., 2023, **21**, 39–52 | **41**

PLQY (in this case the ICT occurs mainly along the C2 arm). A bathochromic shift was also achieved when the C2 arm was left unsubstituted (**9c**) or substituted with an electron-withdrawing trifluoromethyl group (**9d**), albeit with a significant increase in the PLQY up to 1.00. In this case, the ICT occured mainly in the C4 and C6 arms and the electron-attracting character of the pyrimidine nucleus was reinforced by the substituent on the C2 arm.

Some arylvinylpyrimidines are also highly luminescent in the solid state, in particular the diphenylamino derivatives. For example, compound **10** exhibits green emission in a thin film ($\Phi_F = 0.18$)[29] and compound **11** emits yellow light in the KBr matrix (Fig. 5).[30]

4. Sensitivity of emission to external stimuli. Applications as fluorescent (bio)sensors

As mentioned above, the photophysical properties of arylvinylpyrimidines have been demonstrated to be particularly sensitive to environmental stimuli, such as changes in polarity, pH, and the presence of metal cations. In this sense, the ease of protonation, complexation, and hydrogen bonding of the electron lone pairs of the nitrogen atoms provides an excellent tool for developing new (bio)sensing applications. We will briefly describe some of the most typical of these approaches throughout this section.

4.1. Polarity

Push–pull luminescent materials are generally characterized by a slight positive absorption solvatochromism and a pronounced positive emission solvatochromism. This red shift of the emission band with increasing solvent polarity can be explained by the stabilization of a highly polar excited state.[31] However, the emission intensity is significantly reduced in
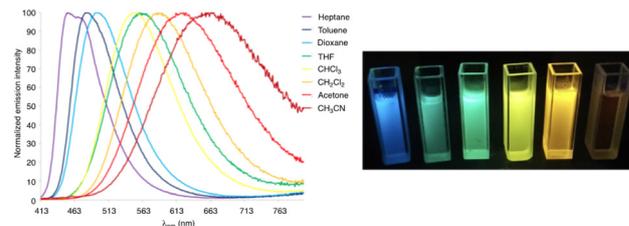
Fig. 6 Left: The normalized emission spectra of compound **11** in a series of aprotic solvents (λ_{exc} = 403 nm). Right: Fluorescence color changes experienced by **11** in various solvents (from left to right: *n*-heptane, toluene, 1,4-dioxane, chloroform, CH$_2$Cl$_2$, and MeCN). The picture was taken in the dark upon irradiation with a UV hand-held lamp (λ_{em} = 366 nm).[30]

more polar solvents. Fig. 6 shows the emission solvatochromism observed for compound **11**.[30] The magnitude of solvatochromism increases considerably with more extended π-conjugated linkers, such as biphenylenevinylene.[32]

4.2. pH

The pyrimidine ring generally acts as a monobasic compound with p$K_a \approx 1.1$ in water.[33] Therefore, it is a weaker base than pyridine (p$K_a \approx 5.2$). After protonation, the electron-withdrawing inductive effect of the resulting quaternary nitrogen drastically reduces the basicity of the second nitrogen atom (second p$K_a \approx -6.3$).[34] For 4-(arylvinyl)pyrimidines, theoretical calculations have shown that protonation occurs almost exclusively at the N1 atom, both in the ground and excited states.[35,36] The protonation of the pyrimidine ring increases its electron-withdrawing character, which enhances the ICT in the push–pull structure and causes a bathochromic shift of the charge transfer absorption band. Fig. 7 illustrates the color change of CH$_2$Cl$_2$ solutions of different compounds **10** and **12** upon the addition of trifluoroacetic acid (TFA). The process is fully reversible.[14]

The protonation of amino-substituted derivatives generally leads to emission quenching,[13,14,16,30,37,38] although in rare exceptions diphenylamino derivatives remain luminescent.[39] Compounds substituted with moderate electron-donating groups, such as methoxy, methyl, or thiomethyl groups, also remain emissive after protonation.[13,14,16,27,37] The gradual
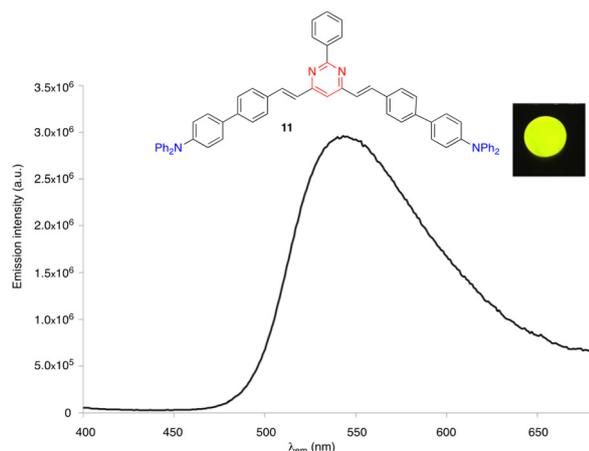

Fig. 5 The solid state emission spectrum of compound **11** embedded into a KBr pellet (3 wt%). Inset: Picture taken in the dark of the KBr pellet upon irradiation with a UV hand-held lamp (λ_{exc} = 366 nm).[30]


Fig. 7 Digital photographs showing the color change experienced by CH$_2$Cl$_2$ solutions of various bis(arylvinyl)pyrimidines **10** and **12** in the presence of 10^{-2} M TFA. Adapted from ref. 14, (copyright 2009, American chemical Society).
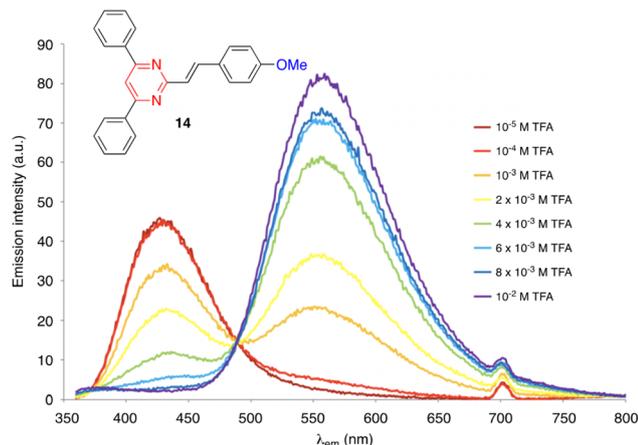
42 | *Org. Biomol. Chem.*, 2023, **21**, 39–52

This journal is © The Royal Society of Chemistry 2023

Fig. 8 Evolution of the emission spectrum of compound **14** (c = 2 × 10^{-6} M) in CH_2Cl_2 solution upon increasing the addition of TFA, excitation at 350 nm. Adapted with permission from ref. 16 (Copyright 2013, Elsevier).

addition of acid leads to the progressive disappearance of both the absorption and emission bands and the appearance of new red-shifted bands corresponding to the protonated forms (Fig. 8). The visible/emission color change is fully reversible by neutralization with a base.

On the other hand, derivatives **15** and **16** (Fig. 9) show null or very little fluorescence in CH_2Cl_2 solution, respectively. However, the presence of acid induces a substantial enhancement in the luminescence response. The absence of emission for **15** can be explained by an excited-state intramolecular proton transfer (ESIPT) from the OH group to the nitrogen atom of the pyrimidine ring.[40] The protonation of the pyrimidine ring by the addition of TFA inhibits the ESIPT process, causing a reversible *switch on* fluorescence response that results in the progressive appearance of a green-yellow emission band (λ_{em} = 550 nm). This acidochromic behavior has also been demonstrated in the solid state by exposure to acid–base vapors. The protonated pyranylidene derivative **16** exhibits a much more intense, blue-shifted emission band compared to the neutral species (λ_{em} = 450 nm, Φ_F = 0.13), which is attributed to the formation of a pyrylium cation after the addition of TFA.[41] Both compounds appear as interesting candidates for anticounterfeiting applications.

Mi and coworkers have recently designed a series of 4,6-distyrylpyrimidine derivatives **17–22** with carbazole substituents (Fig. 10).[42] These compounds self-assemble into organogels (in toluene/xylene/mesitylene for **17**, **19**, and **20**, and DMF/1,4-
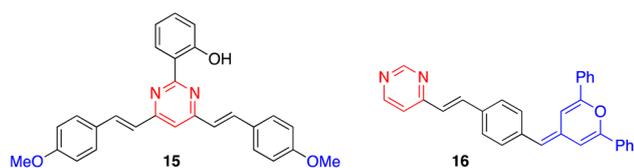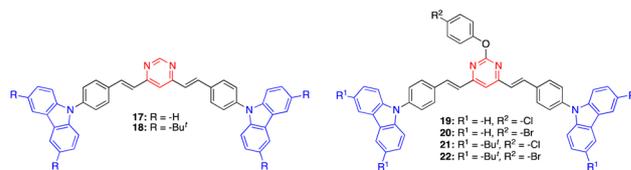
dioxane for **18**, **21**, and **22**) and exhibit an intense emission. The addition of TFA destroys the organogel structure and quenches the emission. A bluish green color emitting xerogel-based film of **18** was described as a TFA vapor sensor with a decay time of 0.6 s and a detection limit of 95 ppb. These high-performance properties are explained by the high surface-to-volume ratio of the nanomaterial and the large space in the 3D network.

Pablos and coworkers have designed polymer membranes that exhibit gel behavior, incorporating proton-sensitive 4,6-distyrylpyrimidine units for the visual detection of the acidity of water at pH below 4 and beyond the pH scale (Fig. 11).[43] The pK_a values of the membranes range from 2.7 to −6.5 in water. Polymer coatings of cotton and other fibers produce smart fabrics that respond colorimetrically to an acid environment, paving the way for fully sensory apparels and smart tags.

4.3. Metal cations

The presence of electron lone pairs on the nitrogen atoms of the pyrimidine ring allow it to complex with metal cations. In this context, arylvinylpyrimidines appear as attractive platforms for the development of fluorescence cation sensors.

Thus, some of us designed a series of 4-arylvinyl-2,6-di (pyridin-2-yl)pyrimidine chromophores that act as tridentate ligands, coordinating a wide variety of metal ions in a similar way to the well-known terpyridine unit.[44] A 1 : 1 stoichiometry was determined for the Zn^{2+} and Sn^{2+} complexes with a remarkably high affinity for Zn^{2+} (greater than terpyridines) (Scheme 3). The coordination leads to a marked bathochromic effect in the absorption spectra and various responses in the emission spectra (*i.e.*, fluorescence quenching or fluorescence intensity enhancement) depending on the metal cation and the arylvinyl moiety. For instance, a noteworthy increase in the emission intensity is observed when Sn^{2+} is added to a THF

Fig. 10 Structure of pyrimidines **17–21**.

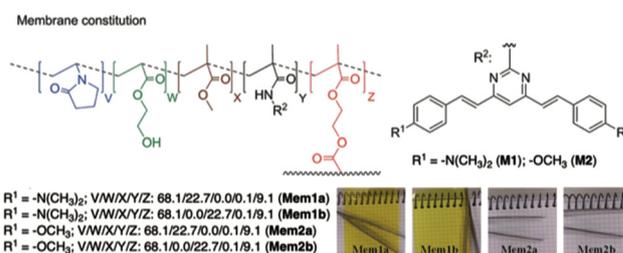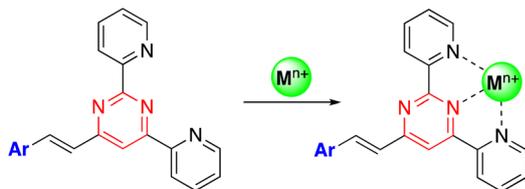**Fig. 9** Structure of derivatives **15** and **16**.

Fig. 11 Structure of the polymer membrane designed by Pablos and coworkers. Reproduced with permission from ref. 43 (copyright 2014, Royal Chemical Society).

This journal is © The Royal Society of Chemistry 2023

Org. Biomol. Chem., 2023, **21**, 39–52 | **43**

Scheme 3 Preparation of metal complexes from of 4-arylvinyl-2,6-di(pyridin-2-yl)pyrimidines.
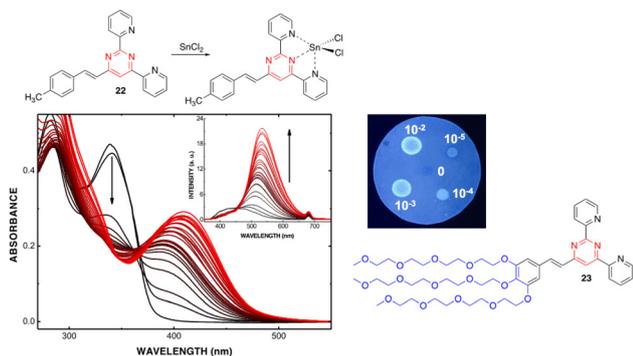

Fig. 12 Left: Changes in the UV/Vis spectrum of **22** (2.0 × 10^{-5} M in THF) upon addition of SnCl$_2$ (from 0 to 7.8 × 10^{-3} M). Inset: Changes in the emission spectrum (excitation at 341 nm). Top right: Spot test to detect Zn^{2+} in aqueous media (10^{-2}–10^{-5} M) using a filter paper disk pretreated with **22**. Bottom right: Water soluble 4-styryl-2,6-di(pyridin-2-yl)pyrimidine **23**. Reproduced with permission from ref. 44 (copyright 2013, Elsevier Limited).

solution of compound **22** (Fig. 12, left). The use of a water-soluble ligand with long polyethylene glycol chains (compound **23**), as well as filter paper disks pretreated with the ligands are various strategies employed for the detection of Zn^{2+}, Ca^{2+}, and Sn^{2+} in aqueous media. In this manner, the Zn^{2+} cation can be detected visually at a concentration as low as 0.6 ppm (10^{-5} M) (Fig. 12, right). Some of these ligands were also incorporated into pluronic nanodots, but this strategy dramatically decreases their sensitivity.[45]

Other exciting derivatives that our group designed and studied were the dipicolylamine (DPA)-substituted styrylpyrimidines **24** and **25** (Fig. 13).[18a] In this type of structure, both the pyrimidine and DPA units can act as metal cation binding sites. In the styrylpyrazine and styrylquinoxaline analogues, the presence of Zn^{2+}, Cd^{2+} or Hg^{2+} leads to a blue shift in the emission. This indicates a decreased ICT in the molecules due
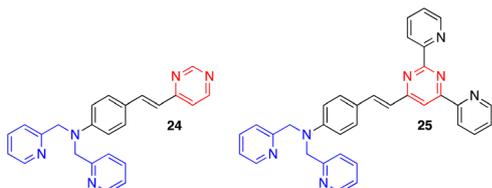
to coordination of the metal cation on the DPA electron-donating group. In contrast, a red shift associated with a substantial quenching of the fluorescence intensity was observed for pyrimidines **24** and **25**, which may be explained by an extra binding of the metal cation on the electron-withdrawing pyrimidine.

Kaur and coworkers have designed chromophores **26** and **27** as colorimetric and highly selective fluorescent probes for the dual detection of Hg^{2+} and Cu^{2+} in aqueous solution (Fig. 14).[46,47] In both systems, the detection of Hg^{2+} is based on the Kucherov reaction on the terminal alkyne grafted at position 2 of the pyrimidine ring, and the detection of Cu^{2+} on the coordination of the metal cation with different hetero-atoms and π-π bonds. While compound **26** exhibits a red shift in the absorption spectra with significant visual color changes and quenching of the fluorescence, compound **27** works as both a colorimetric and ratiometric fluorescence probe (Fig. 15). The detection limits (18 × 10^{-9} M for Hg^{2+} and 21 × 10^{-9} M for Cu^{2+}) are sufficiently low to allow fluorogenic detection at nanomolar concentrations. In addition, solid-state sensors on silica and filter paper were also developed.

Zhang and coworkers reported that styrylpyrimidines **28** and **29** show strong fluorescence quenching and good ratiometric responses towards Cu^{2+} and Fe^{3+}, respectively. The two-photon fluorescence is reversible by the subsequent addition of ethylenediaminetetraacetic acid (EDTA), which allow the use of these pyrimidines as sensitive probes to selectively detect Cu^{2+} and Fe^{3+} in live cells without interference from other
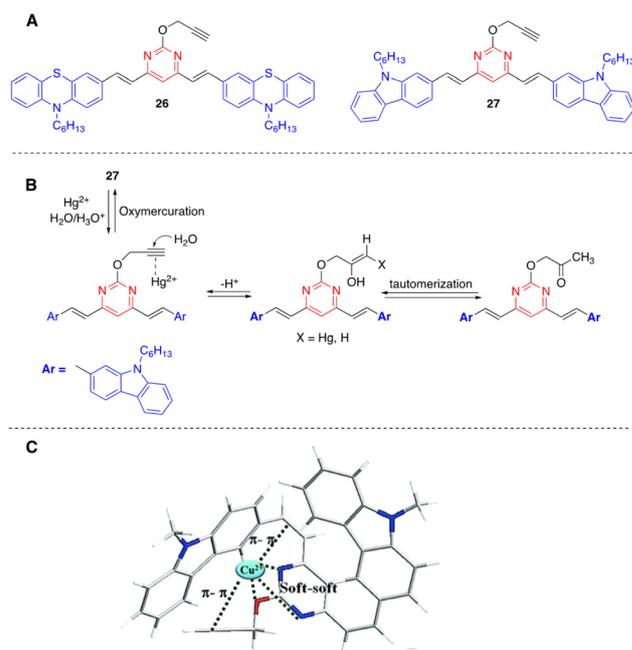

Fig. 13 Structure of dipicolylamine styrylpyrimidines **24** and **25**.

Fig. 14 Structure of Hg^{2+}/Cu^{2+} fluorescence sensors **26** and **27** (A), proposed mechanism for the hydration of probe **27** in the presence of Hg^{2+} (B), and proposed coordinating sites in probe **27** for Cu^{2+} (C). Adapted with permission from ref. 47 (Copyright 2015, Royal Chemical Society).
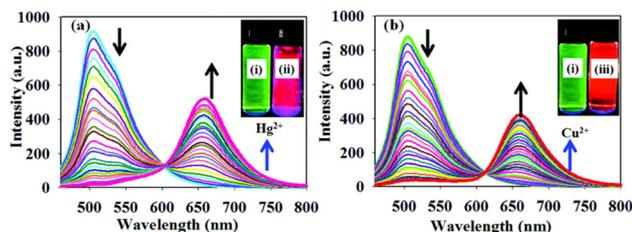
44 | *Org. Biomol. Chem.*, 2023, **21**, 39–52

This journal is © The Royal Society of Chemistry 2023

Fig. 15 Fluorescence spectra of probe **27** (1.0 μM) THF−HEPES buffer (v/v, 7 : 3, pH 7.4) upon incremental addition of (a) Hg^{2+} (0.01−2 equivalents) and (b) Cu^{2+} (0.01−2 equivalents). Inset: Images showing the emission colors of (i) probe **27**, (ii) probe **27** with Hg^{2+}, and (iii) probe **27** with Cu^{2+} under UV light irradiation. Adapted with permission from ref. 47 (Copyright 2015, Royal Chemical Society).
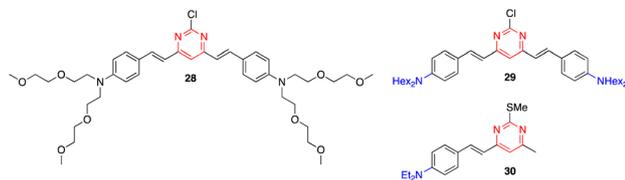

Fig. 16 Structure of styrylpyrimidines **28–30** used as Cu^{2+}/Fe^{3+} fluorescence sensors.

metal ions (Fig. 16).[48] Previously, the same team had described another styrylpyrimidine (compound **30**) that could also be used as an ON–OFF fluorescent probe for the *in vivo* detection of Cu^{2+} (Fig. 16).[49]

4.4. Nitroaromatic explosives

The detection of nitroaromatic explosives by fluorescence quenching has been extensively developed in the context of homeland security and different azaheterocyclic push–pull systems have been designed for such an application.[50]

The detection of low volatile 2,4,6-trinitrotoluene (TNT) is typically based on the contamination of this material by the more volatile 2,4-dinitrotoluene (DNT). Compounds **10** and **31** (Fig. 17, left) are strongly emissive molecules in solution that exhibit a similar moderate PLQY in spin-cast films (Φ_F = 0.18 for **10**, Φ_F = 0.22 for **31**). Exposure to DNT vapors leads to a strong decrease in the emission response of the film.[29] However, the real-time sensing dynamics are strikingly different. While the initial fluorescence signal of **10** decreases by 50% after 430 s, it only takes 13 s for compound **31** (more than one order of magnitude faster) (Fig. 17, right). The incorporation of a long flexible chain into the structure creates a more porous thin film that allows a better penetration of DNT vapors into the material, which explain the faster kinetics observed.

4.5. Hydrogen sulfide

Wang and coworkers developed the biocompatible, non-luminescent styrylpyrimidine probe **32** for the recognition of exogenous/endogenous H_2S at the cellular level.[51] Upon the
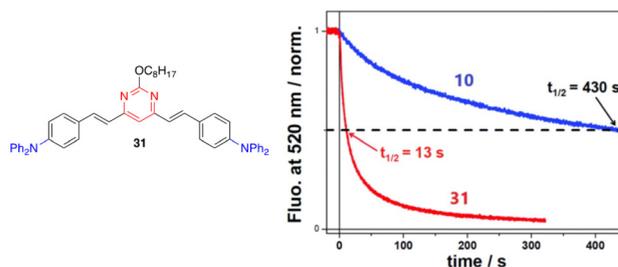

Fig. 17 Left: Structure of styrylpyrimidine **31**. Right: Time-dependent fluorescence intensity of compounds **10** and **31** in films of similar thicknesses (40 ± 5 Å) upon exposure to a N_2 flow of 300 mL min^{-1} with DNT at a vapor pressure of ∼60 ppb. The half-time for fluorescence decay is also indicated for each film. Reproduced with permission from ref. 29 (Copyright 2019, Royal Chemical Society).

addition of H_2S, compound **32** underwent thiolytic cleavage to generate the highly luminescent derivative **33** with excellent selectivity, high sensitivity, and a low detection limit of 3.81 μM in buffered media (Scheme 4). More importantly, **32** can precisely accumulate in the endoplasmic reticulum and holds great potential for tracking endogenous H_2S in various physiological and pathological processes.

4.6. Biomolecules

Aryvinylpyrimidine fluorophores have also found application in the detection of biomolecules. The *N*-methylpyrimidinium derivative **34** is not fluorescent in aqueous media but shows good affinity for double-stranded DNA (DrewAT). Binding to DNA results in a strong bathochromic shift and increased emission (F/F_0 = 35) (Fig. 18).[39]

On the other hand, a series of amino-substituted 4,6-distyrylpyrimidine derivatives **5** and **35–38** have been designed for the *in vitro* detection of a disease-associated protein deposit in the human brain tissue by fluorescence microscopy (Fig. 3 and 19).[19] Compounds **5** and **38** showed significantly higher selectivity for aggregated tau protein over β-amyloid peptides, allowing the selective imaging of tau. Moreover, the ability of **5** to pass the blood–brain barrier was demonstrated and used to detect tau aggregates in Bowman's glands of the olfactory epithelium.

Yang and coworkers designed the OFF–ON fluorescent probe **39**, which exhibits a highly sensitive and selective fluorescence response to NAD(P)H quinone oxidoreductase-1 (NQO1, also known as DT-diaphorase). In the presence of NQO1, a metabolizing enzyme overexpressed in many solid
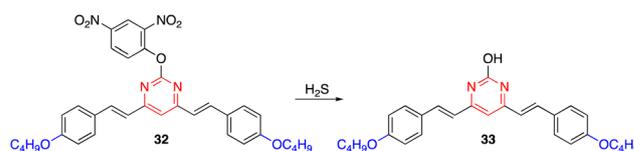
Scheme 4 Thiolytic cleavage of probe **32** to generate luminescent chromophore **33** upon exposure to H_2S.
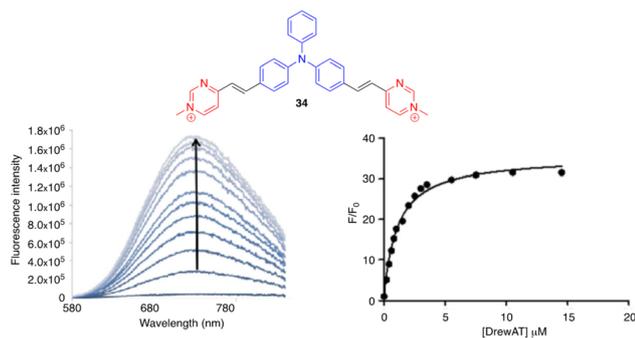
This journal is © The Royal Society of Chemistry 2023

Org. Biomol. Chem., 2023, **21**, 39–52 | **45**

Fig. 18 Left: Fluorometric titration of DrewAT with compound **34** (*c* = 2 μM in 10 mM lithium cacodylate buffer pH 7.2, 100 mM NaCl, [drewAt] = 0−15 μM). Right: Fluorescence enhancement of **34** upon the addition of drewAT. Reproduced with permission from ref. 39 (Copyright 2013, Elsevier Limited).
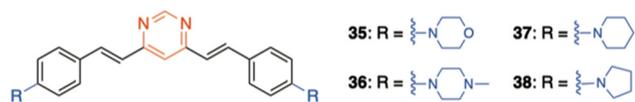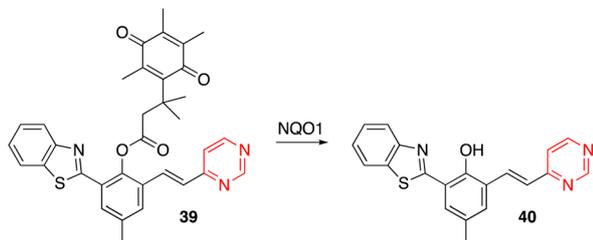

Fig. 19 Structure of 4,6-distyrylpyrimidines **35−38**.

Scheme 5 Cleavage of the quinone propionic acid group of **39** in the presence of NQO1 leading to the luminescent arylvinylpyrimidine **40**.

tumors, the quinone propionic acid group is cleaved, giving rise to the luminescent chromophore **40** (Scheme 5).[52] Probe **39** was successfully applied in detecting endogenous NQO1 in living cancer cells.

5. Dual panchromatic emission

Significant differences in the photophysical behavior of acridan-substituted arylvinylpyrimidines **41** and **42** have been revealed (Fig. 20, top).[53] Diphenylamino derivatives **41c** and **42c** showed classic positive emission solvatochromism, whereas dual emission was observed for methoxy derivatives **41a–b** and **42a–b** in polar solvents. This dual emission consisted of a broad red-shifted band emitted from a state with ICT or twisted ICT nature and a blue-shifted band attributed to a locally excited state. The acridan moiety is completely isolated and does not affect the fundamental absorption properties. The methoxy derivatives also exhibit aggregation-induced emission in mixtures of THF/water, as well as white-
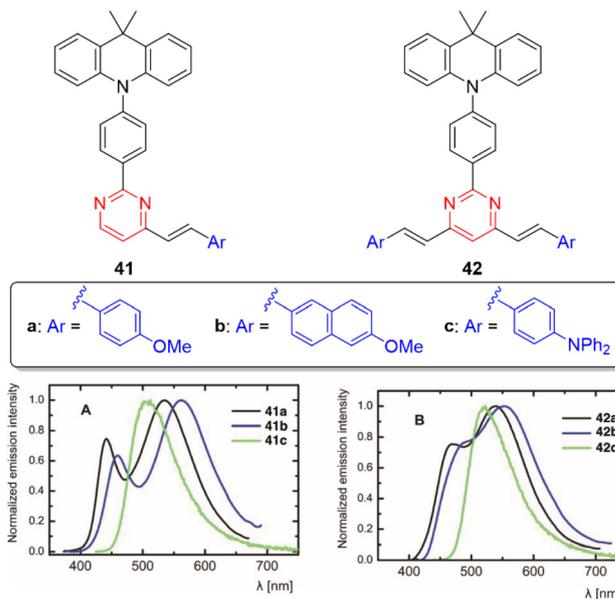

Fig. 20 Top: Structure of the acridan-substituted arylvinylpyrimidines **41** and **42**. Bottom: Emission spectra of neat thin film of **41** and **42**. Adapted with permission from ref. 53 (Copyright 2021, Wiley).

light dual emission in thin films (Fig. 20, bottom), rendering these materials highly promising for the development of white organic light-emitting diodes (WOLEDs). Likewise, the controlled protonation of some blue-emitting arylvinylpyrimidine derivatives leads to dual panchromatic emission with chromaticity coordinates close to pure white light, both in solution and in the solid state.[34,36]

6. Multimodal switches

The diphenylamino-substituted styrylpyrimidine **43** has been designed as a bimodal molecular switch (Scheme 6).[54] Upon addition of HCl or an oxidizing agent such as NOSbF$_6$, a progressive decrease in the absorption band at 399 nm associated with the appearance of a new red-shifted band at 503 nm was observed. One equivalent of oxidizing agent and 10 equivalents of HCl were required for the complete transformation of the system, which can be reversed by two different stimuli. The
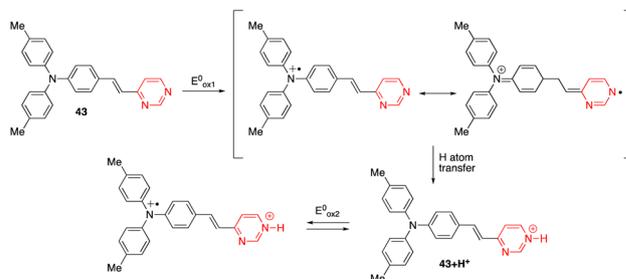
Scheme 6 Proposed route to explain the formation of the protonated form of compound **43** under an electrochemical stimulation.
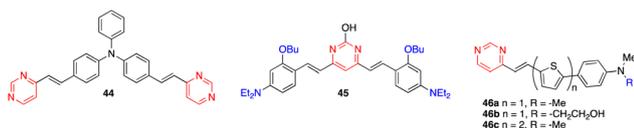
46 | *Org. Biomol. Chem.*, 2023, **21**, 39–52

This journal is © The Royal Society of Chemistry 2023

Fig. 21 Structures of chromophores **44–46**.

initial spectrum could be restored by adding a well-known reducing agent such as hydrazine hydrate or a base such as triethylamine. On the other hand, a redox potential of ∼0.3 V (*vs.* Fc/Fc$^+$) also induced the same changes in the absorption spectrum as chemical oxidation. This result may be explained by the pathway proposed in Scheme 6, which consists of an oxidative cascade initiated with the formation of a radical cation that after abstraction of a hydrogen atom from the surrounding medium gives the corresponding protonated form **43+H$^+$** in an irreversible process. When a potential higher than 0.5 V (*vs.* Fc/Fc$^+$) was applied, a second anodic process assigned to the reversible oxidation of the triphenylamino core was observed. Analogously, the chemical oxidation of compound **44** (Fig. 21) led successively to the corresponding monoprotonated and diprotonated forms, allowing its absorption maximum to switch from the near-UV to the visible, and finally to almost the near-IR region.

7. Photocatalysis

Zhuang and coworkers designed 4,6-arylvinylpyrimidine **45**/graphitic carbon nitride (g-C$_3$N$_4$) nanocomposites for photocatalysis (Fig. 21).[55] The **45**/g-C$_3$N$_4$ photocatalyst with 1 wt% of **45** exhibits the highest photocatalytic activity for the degradation of rhodamine solution under irradiation with visible light. It was reported that the introduction of the arylvinylpyrimidine derivative **45** into the nanomaterial structure promoted interfacial charge transfer and decreased photoinduced electron–hole recombination, thus improving the photocatalytic performance.

8. Dye-sensitized solar cells

Azines, including pyrimidine, have been used as alternative anchoring groups for dye-sensitized solar cells.[56] In this context, the thienylenevinylene pyrimidine derivatives **46** were recently described as light harvesting units (Fig. 21).[57] In this series, the chromophore **46c** exhibits the highest power conversion efficiency with η = 6.4%.

9. Two-photon absorption

Two-photon absorption (TPA) is a third order nonlinear optical (NLO) phenomenon where two photons are absorbed simultaneously upon laser excitation, each with half of the corresponding one-photon absorption energy. TPA is effectively restricted to the focal volume of the laser beam and allows excitation in the biological window of tissues between 700 and 1100 nm. The TPA efficiency is quoted as a two-photon cross section (δ), mostly presented in Göppert-Mayer units (1 GM = 10^{-50} cm^4 s per photon). A large library of NLO chromophores based on pyrimidine have been reported and fundamental structure–property relationships have been recently reviewed and discussed.[58]

The effect of branching on the TPA properties has been investigated in the diphenylamino-substituted styrylpyrimidine series.[59] An increase of the TPA cross section was observed when going from monostyrylpyrimidine **47**, to distyrylpyrimidine **10**, and tristyrylpyrimidine **9a** (Fig. 22). Nevertheless, the regions of linear and non-linear optical spectra of the two and three branched chromophores are similar. Unlike the vast majority of existing branching systems, compound **9a** does not have a $C3$ symmetry, which enhances the TPA response while maintaining the spectral position.

On the other hand, the octupolar D(–π-A)$_3$ arylvinylpyrimidines **48** and **49** with a triphenylamine central core (Fig. 23) were characterized by a moderate TPA cross section (256 GM at 760 nm and 427 GM at 800 nm in CH$_2$Cl$_2$, respectively) and PLQY > 0.5.[60]

Tetrastyrylpyrimidines **50** and **51** and the fluorene analogue **52** were characterized by TPA cross sections ranging from 460 to 1022 GM in THF at 775–790 nm (Fig. 24).[15] Complexation with Zn^{2+} with **50** and **51** induces a planarization of the structure with a decrease and red shift of TPA cross sections. In contrast, a divergent effect was observed for the complex of the fluorene analogue **52** as the 3D structure is maintained, inducing a marked increase in the TPA cross section up to 2000 GM.
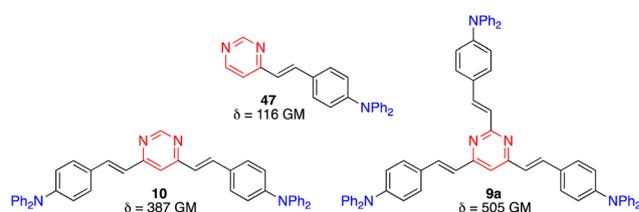

Fig. 22 TPA cross sections in CH$_2$Cl$_2$ of diphenylamino-substituted styrylpyrimidine derivatives **9a**, **10**, and **47**.
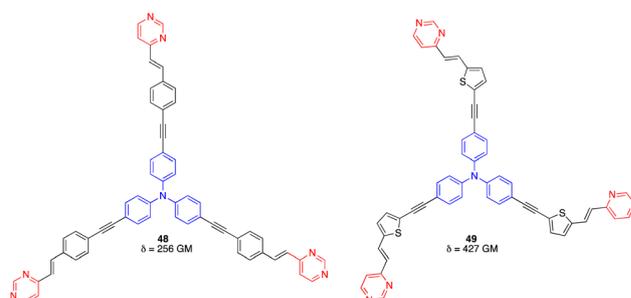

Fig. 23 Structures of octupolar arylvinylpyrimidines **48** and **49**.

This journal is © The Royal Society of Chemistry 2023

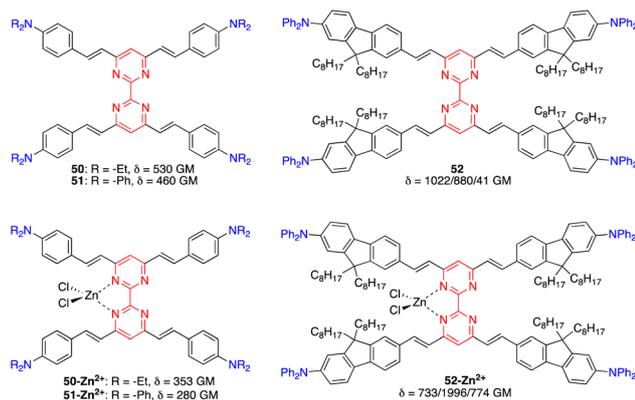*Org. Biomol. Chem.*, 2023, **21**, 39–52 | **47**

Fig. 24 Structures of bipyrimidine chromophores **50–52**.

In the following subsections, we will highlight some key applications of selected materials.

9.1. Bioimaging

Due to their significant TPA cross sections (several hundred GM) and high PLQYs, many amino-substituted 4,6-distyrylpyrimidines have been used for bioimaging applications. The required water solubility, if necessary, can be provided by functionalizing the styrylpyrimidine scaffold. Various 4,6-distyrylpyrimidines TPA fluorophores, such as **53–57**, stain the cytoplasmic region of cells (Fig. 25, top).[23a,b,61] On the other hand, chromophores **58** with hexafluorophosphate water-solubilizing groups revealed to be mitochondrial targeting probes,[62] while chromophores **59** and **60** target the endoplasmic reticulum (Fig. 25, bottom).[63]

The 4,6-distyrylpyrimidine **61** was designed as a TPA OFF–ON fluorescent probe to monitor the phosphatase activity in cells and tissues (Scheme 7).[64] The hydroxyl group at the C2 position of the pyrimidine ring can be used for conjugation with different cell-penetrating peptides, allowing organelle- and tumor cell-specific imaging of phosphatase activities in both live mammalian cells and Drosophila brains.
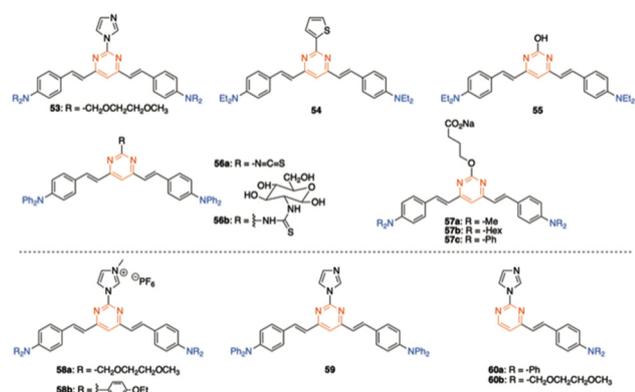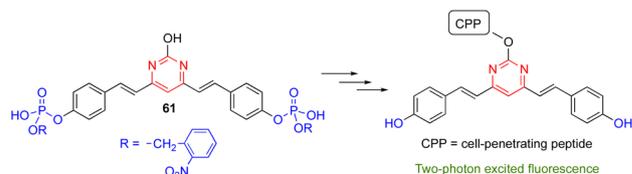

Scheme 7 Distyrylpyrimidine **61** as the OFF–ON probe to monitor phosphatase activity.

9.2. Data storage

Li and coworkers reported the 4,6-distyrylpyrimidine **62**, which combines a noteworthy TPA cross section, broad TPA band throughout the whole 700–900 nm range, and high fluorescence quantum yield (Fig. 26). Such compound is of particular interest for optical storage in the visible and NIR regions when it is used as a dopant photoinitiator in poly (methyl methacrylate) films.[20b]

9.3 Optical limiting

Wang and coworkers designed compound **63** for optical power limiting, in which a cooperative effect between the porphyrin and the di(arylvinyl)pyrimidine fragment was demonstrated (Fig. 26).[65] The enhanced optical limiting properties were ascribed to a combination of excited-state absorption, reverse saturable absorption, non-linear refraction, and fluorescence resonance energy transfer from the pyrimidine chromophore to the porphyrin core.

9.4. Microfabrication

Malval and coworkers described a new conjugated oligomer **64**, which has alternating vinylpyrimidine and triphenylamine subunits (Fig. 27).[26] Size exclusion chromatography, NMR analyses, and DFT calculations have shown that this oligomer consists of 8 to 10 units and exhibits a highly distorted geometry, resulting in a weak interchromophore coupling within the oligomer and strong reduction of the effective conjugation length. This explains why the absorption and emission properties resemble those measured for its 4,6-distyrylpyrimidine monomer **10**. Nevertheless, **61** shows a larger TPA cross section (δ = 5093 GM at 800 nm) than **10** (δ = 360 GM). This very high TPA ability has been aimed to improve the TPA-induced polymerization efficiency of a bicomponent photoinitiator system for microfabrication (Fig. 27).

Fig. 25 Structures of different amino-substituted 4,6-distyrylpyrimidines used in bioimaging.

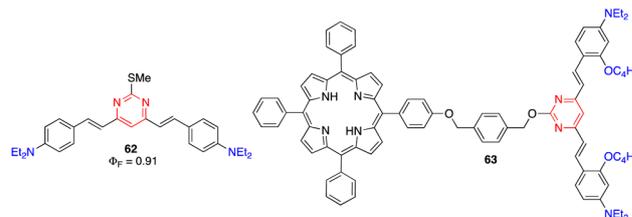**Fig. 26** Structures of arylvinylpyrimidines **62** and **63** used for data storage and optical power limiting applications, respectively.

48 | *Org. Biomol. Chem.*, 2023, **21**, 39–52

This journal is © The Royal Society of Chemistry 2023

Fig. 27 Top left: Structure of the oligomer **64**. Top right: SEM image of a μ-structure fabricated upon excitation at 800 nm of a diacrylate resin with **64** as the TPA sensitizer. Inset: 2D model master. Bottom: Optimized geometries of **64** associating three monomer units (PBE0/6-31G(d) level). Adapted with permission from ref. 26 (Copyright 2013, Royal Chemical Society).

10. Second order NLO chromophores

Another common feature of non-centrosymmetric organic push–pull derivatives is their second-order NLO properties that specifically lead to sum frequency generation, including second harmonic generation (SHG),[66] Pockels effect, and optical rectification,[67] all of which have found application in optical signal processing and integrated optics.[68] The second-order NLO properties can be estimated in solution using the electric-field induced second harmonic generation (EFISH) method at a non-resonant incident wavelength of 1907 nm. The EFISH method is based on the application of a high external electric field $\vec{E}$ on the analytical cell to align the chromophores in the same direction. With this method, the NLO response is determined as the scalar product between the permanent dipole moment of the molecule $\vec{\mu}$ and the vector component $\beta_{//}$ of its hyperpolarizability tensor β. The results can be influenced by resonance phenomena and a corrected value of $\mu\beta_0$ according to the two-state model better representing the real NLO response.[69]

Due to the modest values shown by classical arylvinylpyrimidines such as **47** ($\mu\beta_0 = 150 \times 10^{-48}$ esu),[13,58] diverse strategies have been employed to enhance the NLO responses. One of them involves the alteration of the π-conjugated linker. Thus, whereas a biphenylene linker does not significantly improve the NLO response (**65**), probably because the conjugation is limited by torsion between the two phenyl rings,[13,70] the incorporation of a triple bond (**66**) and the replacement of one phenylene by a thienylene moiety (**67**) enhance the NLO response (Fig. 28).[17] The use of proaromatic pyranylidene groups in the structures of the styrylpyrimidine **16** ($\mu\beta_0 = 300 \times 10^{-48}$ esu) and the 4,6-distyrylpyrimidine **68** ($\mu\beta_0 = 480 \times 10^{-48}$ esu) positively influences the NLO response.[71] Nevertheless,
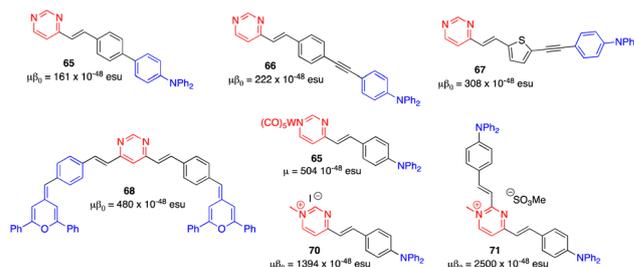

Fig. 28 Structures and NLO responses of compounds **65–71**.

the most efficient way to increase the value of $\mu\beta_0$ is to reinforce the electron-withdrawing character of the pyrimidine ring by complexation with tungsten pentacarbonyl (**69**) or methylation at the N1 atom (**70**).[72] The latter leads to a value of $\mu\beta_0$ around 9 times higher ($\mu\beta_0 = 1394 \times 10^{-48}$ esu) than that of the reference chromophore **47**. The chromophore **71**, with a 2,4-disubstituted methylated pyrimidinium core, exhibits the highest $\mu\beta_0$ value in the series (2500×10^{-48} esu).[73]

Organometallic derivatives **72–74**, in which a metallic center (Pt or Ru) is incorporated into the π-conjugated structure, show particularly high $\mu\beta_0$ values of up to 6000×10^{-48} esu for the ruthenium complex **74** (Fig. 29).[74,75]

Akdas-Kiliç and coworkers have designed a series of tetra (arylvinyl)bipyrimidines **75** with long alkoxyl chains (Fig. 30).[76,77] Compounds **75a** and **75b** with C_{12} and C_{16} chains exhibit mesomorphic as well as second-order NLO properties in solution ($\beta_0 = 38$–42×10^{-30} esu, measured by hyper-Rayleigh scattering in CH_2Cl_2). Nevertheless, they are SHG silent in their liquid crystalline phases due to the formation of columnar mesophases with hexagonal symmetry. In contrast, grafting of branched chiral alkyl chains (**75c**) leads to right- or left-handed twisted columnar structures depending on the chirality of the side chains. This strategy allows translation of

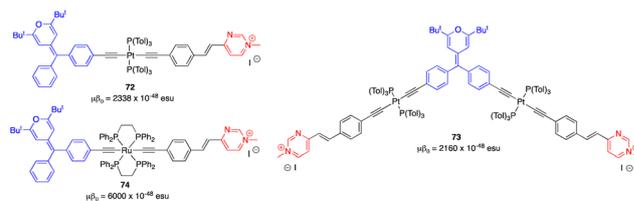

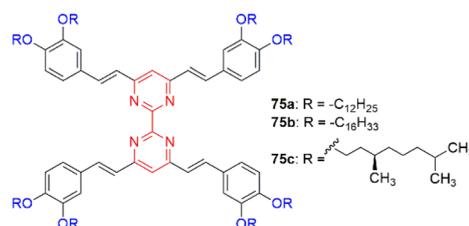Fig. 29 Structures and NLO responses of organometallic compounds **72–74**.

Fig. 30 Structures of tetra(arylvinyl)bipyrimidines **75**.

This journal is © The Royal Society of Chemistry 2023

Org. Biomol. Chem., 2023, **21**, 39–52 | **49**

the NLO response from molecular level to the bulk level as shown by SHG measurements.

11. Conclusions

This article has provided a general overview of the main strategies for the synthesis of arylvinylpyrimidines, as well as highlighting their interesting photophysical properties. Specifically, these compounds are typically prepared by the Knoevenagel condensation of aromatic aldehydes with methylpyrimidine derivatives. This methodology is the most suitable because of a wide range of commercially available starting materials, the use of environmentally friendly conditions in most cases, the easy treatment of crude reaction mixtures, and the high control of the stereochemistry.

All these molecules display extraordinary optical properties, although they generally must be substituted with electron-donating amino or alkoxy groups to show significant emission. The final luminescence properties strongly depend on the substitution at pyrimidine and aryl moieties and are particularly sensitive to environmental stimuli, which provides an excellent tool for developing new sensing and optoelectronic devices. Nowadays, the main interest in this area is focused on addressing the needs of the industry and overcoming the difficulties of implementing the material in real devices, which is still a major challenge.

Conflicts of interest

There are no conflicts to declare.

Acknowledgements

References

1 F. Bureš, RSC Adv., 2014, 4, 58826–58851.

2 L. Beverina and G. A. Pagani, Acc. Chem. Res., 2014, 47, 319–329.

3 (a) A. Pal, M. Karmakar, S. R. Bhatta and A. Thakur, Coord. Chem. Rev., 2021, 448, 214167; (b) E. V. Verbitskiy, G. L. Rusinov, O. N. Chupakhin and V. N. Charushin, Dyes Pigm., 2020, 180, 108414.

4 (a) M. Y. Wong and E. Zysman-Colman, Adv. Mater., 2017, 29, 1605444; (b) J. Lee, K. Shizu, H. Tanaka, H. Nomura, T. Yasuda and C. Adachi, J. Mater. Chem. C, 2013, 1, 4599–4604.

5 H. Moon, W. S. Jahng and M. D. Curtis, J. Mater. Chem., 2008, 18, 4856–4863.

6 (a) J.-M. Ji, H. Zhou and H. K. Kim, J. Mater. Chem. A, 2018, 6, 14518–14545; (b) V. Malytskyi, J.-J. Simon, L. Patrone and J.-M. Raimundo, RSC Adv., 2015, 5, 354–397; (c) W. Li, L. Ye, S. Li, H. Yao, H. Ade and J. Hou, Adv. Mater., 2018, 30, 1707170.

7 G. S. He, L.-S. Tan, Q. Zheng and P. N. Prasad, Chem. Rev., 2008, 108, 1245–1330.

8 J. Liu, C. Ouyang, F. Huo, W. He and A. Cao, Dyes Pigm., 2020, 181, 108509.

9 S. Achelle, J. Rodríguez-López and F. Robin-le Guen, ChemistrySelect, 2018, 3, 1852–1886.

10 (a) S. Achelle and N. Plé, Curr. Org. Synth., 2012, 9, 163–187; (b) G. N. Lipunova, E. V. Nosova, V. N. Charushin and O. N. Chupakhin, Curr. Org. Synth., 2018, 15, 793–814; (c) R. Komatsu, H. Sasabe and J. Kido, J. Photonics Energy, 2018, 8, 032108.

11 G. A. Molander and C. R. Bernardi, J. Org. Chem., 2002, 67, 8424–8429.

12 (a) J.-J. Vanden Eynde, L. Pascal, Y. Van Haverbeke and P. Dubois, Synth. Commun., 2001, 31, 3167–3173; (b) L. Pascal, J.-J. Vanden Eynde, Y. Van Haverbeke, P. Dubois, A. Michel, U. Rant, E. Zojer, G. Leising, L. O. Van Dorn, N. E. Gruhn, J. Cornil and J.-L. Brédas, J. Phys. Chem. B, 2002, 106, 6442–6450.

13 S. Achelle, A. Barsella, C. Baudequin, B. Caro and F. Robin-le Guen, J. Org. Chem., 2012, 77, 4087–4096.

14 S. Achelle, I. Nouira, B. Pfaffinger, Y. Ramondenc, N. Plé and J. Rodríguez-López, J. Org. Chem., 2009, 74, 3711–3717.

15 P. Savel, H. Akdas-Kiliç, J.-P. Malval, A. Spangenberg, T. Roisnel and J.-L. Fillaut, J. Mater. Chem. C, 2014, 2, 295–305.

16 S. Achelle and F. Robin-le Guen, Tetrahedron Lett., 2013, 54, 4491–4496.

17 S. Achelle, A. Barsella, B. Caro and F. Robin-le Guen, RSC Adv., 2015, 5, 39218–39227.

18 (a) S. Achelle, J. Rodríguez-López, F. Bureš and F. Robin-le Guen, Dyes Pigm., 2015, 121, 305–311; (b) G. Khalil, C. Orvain, L. Fang, L. Barloy, A. Chaumont, C. Gaiddon, M. Henry, N. Kyritsakas and P. Mobian, Dalton Trans., 2016, 45, 19072–19085; (c) H. Akdas-Kiliç, T. Roisnel, I. Ledoux and H. le Bozec, New J. Chem., 2009, 33, 1470–1473.

19 A. Boländer, D. Kieser, C. Voss, S. Bauer, C. Schön, S. Burgold, T. Bittner, J. Hölzer, R. Heyny-von Haußen, G. Mall, V. Goetschy, C. Czech, H. Knust, R. Berger, J. Herms, I. Hilger and B. Schmidt, J. Med. Chem., 2012, 55, 9170–9180.

20 (a) F.-A. Martin, C. Baudequin, C. Fiol-Petit, M. Darabantu, Y. Ramondenc and N. Plé, Tetrahedron, 2014, 70, 2546–2555; (b) L. Li, Y.-P. Tian, J.-X. Yang, P.-P. Sun, J.-Y. Wu, H.-P. Zhou, S.-Y. Zhang, B.-K. Jin, X.-J. Xing, C.-K. Wang, M. Li, G.-H. Cheng, H.-H. Tang, W.-H. Huang, X.-T. Tao and M.-H. Jiang, Chem. – Asian J., 2009, 4, 668–680.

21 M. Klikar, P. le Poul, A. Růžička, O. Pytela, A. Barsella, K. D. Dorkenoo, F. Robin-le Guen, F. Bureš and S. Achelle, J. Org. Chem., 2017, 82, 9435–9451.

50 | Org. Biomol. Chem., 2023, 21, 39–52

This journal is © The Royal Society of Chemistry 2023

22 A. A. Parent, D. H. Ess and J. A. Katzenellenbogen, *J. Org. Chem.*, 2014, **79**, 5448–5462.

23 (*a*) H. Wang, Q. Zhang, J. Zhang, L. Li, Q. Zhang, S. Li, S. Zhang, J. Wu and Y. Tian, *Dyes Pigm.*, 2014, **102**, 263–272; (*b*) B. Liu, H.-L. Zhang, J. Liu, Y.-D. Zhao, Q.-M. Luo and Z.-L. Huang, *J. Mater. Chem.*, 2007, **17**, 2921–2929.

24 S. Achelle, L. Bodiou, J. Charrier and F. Robin-le Guen, *C. R. Chim.*, 2016, **19**, 279–285.

25 S. S. Gunathilake, H. D. Magurudeniya, P. Huang, H. Nguyen, E. A. Rainbolt, M. C. Stefan and M. C. Biewer, *Polym. Chem.*, 2013, **4**, 5216–5219.

26 J.-P. Malval, S. Achelle, L. Bodiou, A. Spangenberg, L. C. Gomez, O. Soppera and F. Robin-le Guen, *J. Mater. Chem. C*, 2014, **2**, 7869–7880.

27 M. Fecková, P. le Poul, F. Robin-le Guen, T. Roisnel, O. Pytela, M. Klikar, F. Bureš and S. Achelle, *J. Org. Chem.*, 2018, **83**, 11712–11726.

28 C. Denneval, S. Achelle, C. Baudequin and F. Robin-le Guen, *Dyes Pigm.*, 2014, **110**, 49–55.

29 J.-P. Malval, M. Cranney, S. Achelle, H. Akdas-Kiliç, J.-L. Fillaut, N. Cabon, F. Robin-le Guen, O. Soppera and Y. Molard, *Chem. Commun.*, 2019, **55**, 14331–14334.

30 L. Diarra, F. Robin-le Guen and S. Achelle, *Molbank*, 2021, M1278.

31 R. Lartia, C. Allain, G. Bordeau, F. Schmidt, C. Fiorini-Debuisschert, F. Charra and M.-P. Teulade-Fichou, *J. Org. Chem.*, 2008, **73**, 1732–1744.

32 S. Achelle and F. Robin-le Guen, *J. Photochem. Photobiol., A*, 2017, **348**, 281–286.

33 R. Milcent, *Chimie Organique Hétérocyclique*, EDP Science, Les Ulis, 2003, p. 605.

34 S. Achelle, J. Rodríguez-López, F. Bureš and F. Robin-le Guen, *Chem. Rec.*, 2020, **20**, 440–451.

35 M. Hodée, A. Lenne, J. Rodríguez-López, F. Robin-le Guen, C. Katan, S. Achelle and A. Fihey, *New J. Chem.*, 2021, **45**, 19132–19144.

36 S. Achelle, J. Rodríguez-López, C. Katan and F. Robin-le Guen, *J. Phys. Chem. C*, 2016, **120**, 26986–26995.

37 C. Hadad, S. Achelle, J. C. García-Martínez and J. Rodríguez-López, *J. Org. Chem.*, 2011, **76**, 3837–3845.

38 F. Kournoutas, I. K. Kalis, M. Fecková, S. Achelle and M. Fakis, *J. Photochem. Photobiol., A*, 2020, **391**, 112398.

39 A. I. Aranda, S. Achelle, F. Hammerer, F. Mahuteau-Betzer and M.-P. Teulade-Fichou, *Dyes Pigm.*, 2012, **95**, 400–407.

40 R. Plaza-Pedroche, M. P. Fernández-Liencres, S. B. Jiménez-Pulido, N. A. Illán-Cabeza, S. Achelle, A. Navarro and J. Rodríguez-López, *ACS Appl. Mater. Interfaces*, 2022, **14**, 24964–24979.

41 S. Achelle, S. Kahlal, J.-Y. Saillard, N. Cabon, B. Caro and F. Robin-le Guen, *Tetrahedron*, 2014, **70**, 2804–2815.

42 W. Mi, Z. Qu, J. Sun, J. Sung, F. Zhang and K. Ye, *Dyes Pigm.*, 2018, **150**, 207–215.

43 J. L. Pablos, P. Estévez, A. Muñoz, S. Ibeas, F. Serna, F. C. García and J. M. García, *J. Mater. Chem. A*, 2015, **3**, 2833–2843.

44 C. Hadad, S. Achelle, I. López-Solera, J. C. García-Martínez and J. Rodríguez-López, *Dyes Pigm.*, 2013, **97**, 230–237.

45 L. Vurth, C. Hadad, S. Achelle, J. C. García-Martínez, J. Rodríguez-López and O. Stéphan, *Colloid Polym. Sci.*, 2012, **290**, 1353–1359.

46 M. Kaur, M. J. Cho and D. H. Choi, *Dyes Pigm.*, 2016, **125**, 1–7.

47 M. Kaur, Y.-H. Ahn, K. Choi, M. J. Cho and D. H. Choi, *Org. Biomol. Chem.*, 2015, **13**, 7149–7153.

48 Q. Zhang, X. Tian, H. Wang, Z. Hu, J. Wu, H. Zhou, S. Zhang, J. Yang, Z. Sun, Y. Tian and K. Uvdal, *Sens. Actuators, B*, 2016, **222**, 574–578.

49 Q. Zhang, L. Li, M. Zhang, Z. Liu, J. Wu, H. Zhou, J. Yang, S. Zhang and Y. Tian, *Dalton Trans.*, 2013, **42**, 8848–8853.

50 E. V. Verbitskiy, G. L. Rusinov, O. N. Chupakhin and V. N. Charushin, *Dyes Pigm.*, 2020, **180**, 108414.

51 H. Wang, L. Hu, B. Xu, H. Chen, F. Cai, N. Yang, Q. Wu, K. Uvdal, Z. Hu and L. Li, *Dyes Pigm.*, 2020, **179**, 108390.

52 Q. Yang, Y. Wen, J. Xu and S. Shao, *Talanta*, 2020, **216**, 120982.

53 M. Fecková, I. K. Kalis, T. Roisnel, P. le Poul, O. Pytela, M. Klikar, F. Robin-le Guen, F. Bureš, M. Fakis and S. Achelle, *Chem. – Eur. J.*, 2021, **27**, 1145–1159.

54 O. Alévêque, S. Achelle and L. Sanguinet, *ChemPhotoChem*, 2022, DOI: **10.1002/cptc.202200201**, in press.

55 J. Zhuang, J. Zhang, J. Pang, A. Wang, X. Wang and W. Zhu, *Dyes Pigm.*, 2019, **163**, 634–640.

56 E. V. Verbitskiy, G. L. Rusinov, O. N. Chupakhin and V. N. Charushin, *Dyes Pigm.*, 2021, **194**, 109650.

57 I. Duerto, S. Sarasa, D. Barrios, J. Orduna, B. Villacampa and M.-J. Blesa, *Dyes Pigm.*, 2022, **203**, 110310.

58 M. Fecková, P. le Poul, F. Bureš, F. Robin-le Guen and S. Achelle, *Dyes Pigm.*, 2020, **182**, 108659.

59 F. Kournoutas, A. Fihey, J.-P. Malval, A. Spangenberg, M. Fecková, P. le Poul, C. Katan, F. Robin-le Guen, F. Bureš, S. Achelle and M. Fakis, *Phys. Chem. Chem. Phys.*, 2020, **22**, 4165–4176.

60 D. Cvejn, S. Achelle, O. Pytela, J.-P. Malval, A. Spangenberg, N. Cabon, F. Bureš and F. Robin-le Guen, *Dyes Pigm.*, 2016, **124**, 101–109.

61 (*a*) Q. Zhang, L. Luo, H. Xu, Z. Hu, C. Brommesson, J. Wu, Z. Sun, Y. Tian and K. Uvdal, *New J. Chem.*, 2016, **40**, 3456–3463; (*b*) C. Tang, Q. Zhang, D. Li, J. Zhang, P. Shi, S. Li, J. Wu and Y. Tian, *Dyes Pigm.*, 2013, **99**, 20–28; (*c*) Q. Zhang, J. Luo, L. Ye, H. Wang, B. Huang, J. Zhang, J. Wu, S. Zhang and Y. Tian, *J. Mol. Struct.*, 2014, **1074**, 33–42; (*d*) J. Yang, W. Hu, H. Li, H. Hou, Y. Tu and B. Liu, *Photochem. Photobiol. Sci.*, 2018, **17**, 474–481.

62 Q. Zhang, R. Guan, X. Tian, L. Luo, H. Zhou, S. Li, J. Wu and Y. Tian, *RSC Adv.*, 2017, **7**, 20068–20075.

63 (*a*) L. Hu, S. Hussain, T. Liu, Y. Yue, J. Liu, Y. Tian and X. Tian, *New J. Chem.*, 2018, **42**, 14725–14728; (*b*) Q. Zhang, X. Tian, Z. Hu, C. Brommesson, J. Wu, H. Zhou, J. Yang, Z. Sun, Y. Tian and K. Uvdal, *Dyes Pigm.*, 2016, **126**, 286–295.

64 L. Li, J. Ge, H. Wu, Q.-H. Xu and S. Q. Yao, *J. Am. Chem. Soc.*, 2012, **134**, 12157–12167.

This journal is © The Royal Society of Chemistry 2023

Org. Biomol. Chem., 2023, **21**, 39–52 | **51**

65 A. Wang, L. Long, S. Meng, X. Li, W. Zhao, Y. Song, M. P. Cifuentes, M. G. Humphrey and C. Zhang, *Org. Biomol. Chem.*, 2013, **11**, 4250–4257.

66 A. Morita, *Theory of sum frequency generation spectroscopy*, Springer Nature Singapore Pte Ltd., 2018.

67 M. Bass, P. A. Franken, J. F. Ward and G. Weinreich, *Phys. Rev. Lett.*, 1962, **9**, 446–448.

68 (*a*) Y. Qi and Y. Li, *Nanophotonics*, 2020, **9**, 1287–1320; (*b*) O.-S. Prelipceanu, M. Prelipceanu, N. Paraschiv, A. Popa and O. Geman, *Symmetry*, 2019, **11**, 60; (*c*) C. Koos, P. Vorreau, T. Vallaitis, P. Dumon, W. Bogaerts, R. Baets, B. Esembeson, I. Biaggio, T. Michinobu, F. Diederich, W. Freude and J. Leuthold, *Nat. Photonics*, 2009, **3**, 216–219; (*d*) D. Cotter, R. J. Manning, K. J. Blow, A. D. Ellis, A. E. Kelly, D. Nesset, I. D. Phillips, A. J. Poustie and D. C. Rogers, *Science*, 1999, **286**, 1523–1528; (*e*) B. Jalali and S. Fathpour, *J. Lightwave Technol.*, 2006, **24**, 4600–4615.

69 D. R. Kanis, M. A. Ratner and T. J. Marks, *Chem. Rev.*, 1994, **94**, 195–242.

70 F. Castet, A. Pic and B. Champagne, *Dyes Pigm.*, 2014, **110**, 256–260.

71 S. Achelle, J.-P. Malval, S. Aloïse, A. Barsella, A. Spangenberg, L. Mager, H. Akdas-Kiliç, J.-L. Fillaut, B. Caro and F. Robin-le Guen, *ChemPhysChem*, 2013, **14**, 2725–2736.

72 S. Achelle, S. Kahlal, A. Barsella, J.-Y. Saillard, X. Che, J. Vallet, F. Bureš, B. Caro and F. Robin-le Guen, *Dyes Pigm.*, 2015, **113**, 562–570.

73 S. Achelle, E. V. Verbitskiy, M. Fecková, F. Bureš, A. Barsella and F. Robin-le Guen, *ChemPlusChem*, 2021, **86**, 758–762.

74 (*a*) R. J. Durand, S. Gauthier, S. Achelle, S. Kahlal, J.-Y. Saillard, A. Barsella, L. Wojcik, N. le Poul and F. Robin-le Guen, *Dalton Trans.*, 2017, **46**, 3059–3069; (*b*) R. J. Durand, S. Achelle, F. Robin-le Guen, E. Caytan, N. le Poul, A. Barsella, P. Guevara Level, D. Jacquemin and S. Gauthier, *Dalton Trans.*, 2021, **50**, 4623–4633.

75 R. J. Durand, S. Gauthier, S. Achelle, T. Groizard, S. Kahlal, J.-Y. Saillard, A. Barsella, N. le Poul and F. Robin-le Guen, *Dalton Trans.*, 2018, **47**, 3965–3975.

76 H. Akdas-Kiliç, M. Godfroy, J.-L. Fillaut, B. Donnio, B. Heinrich, P. Kędziora, J.-P. Malval, A. Spangenberg, S. van Cleuvenbergen, K. Clays and F. Camerel, *J. Phys. Chem. C*, 2015, **119**, 3697–3710.

77 S. van Cleuvenbergen, P. Kędziora, J.-L. Fillaut, T. Verbiest, K. Clays, H. Akdas-Kiliç and F. Camerel, *Angew. Chem., Int. Ed.*, 2017, **56**, 9546–9550.